Chapter 9

Viscoplastic Behaviour of Polyamides

Şerban Dan-Andrei

Additional information is available at the end of the chapter

http://dx.doi.org/10.5772/64563

Abstract

In this study, the viscoplastic behaviour of a polyamide-based thermoplastic polymer was investigated by performing a number of tests that highlighted the influence of time and temperature on the mechanical behaviour: strain-rate- and temperature-dependency tests, creep tests, dynamic mechanical analysis (DMA) tests, Mullins' effect tests, and low-cycle fatigue tests. The results are discussed and explanations are proposed regarding the particularities the investigated material exhibits during deformation.

Keywords: viscoplasticity, polyamide, thermoplastic polymers

1. Introduction

When designing assemblies for engineering applications, the material characteristics of various components are often considered to be characterized only by simple laws, such as linear elasticity and plasticity for solids and viscosity for fluids. In reality, all materials exhibit both elasticity and viscosity during deformation [1]. The elastic behaviour of fluids is often characterized by the bulk modulus, a measure of its stiffness during hydrostatic compression [2]. Viscous effects in solids can be observed in various loading scenarios, the most common being strain-rate dependency, temperature dependency and creep [3]. Although rarely taken into account for metals or concretes, viscous effects play a major part in defining the mechanical response of polymers [1, 4–6]. Their characteristic structure of long, covalently bonded chains of atoms, with very high molecular weights, is responsible for the mechanisms of inducing temporary damage, such as viscous flow, bond interchange, Thirion relaxation, etc. [2].

Throughout human history, polymers were used for a great variety of purposes. Natural polymers, such as cotton, silk, wool and resins, were employed for various household purposes

as far back as 6000 years ago [5]. The extensive use of synthetic polymers began in the 1940s. Their advantages over conventional materials (metals, wood, textiles, etc.), namely low specific mass for fairly good mechanical properties, low production costs and good insulation properties, determined an exponential increase in the number of applications. For the past 20 years, the total production of polymers exceeded the combined metal production volume wise [5].

The unique time- and temperature-dependent properties of rubbers were observed and described by various scientists of the nineteenth century. Ludwig Boltzmann (the first to coin the term viscoelasticity), James Clerk Maxwell, Sir William Thompson and Lord Kelvin were the first to provide mathematical models in describing viscoelasticity [5]. Today, the basic models developed by the aforementioned scientist (the Maxwell fluid, the Kelvin solid coupled with the Boltzmann superposition principle) represent the backbone of various advanced models used in describing the mechanical behaviour of viscoelastic and viscoplastic materials [5, 6].

Breaking down the behaviour of viscoelastic materials into the solid-like and fluid-like response, several constitutive formulations can be considered. The elastic part is usually described by Hookean elasticity for brittle polymers (linear elastic response) and by various non-linear models for more compliant materials [5, 6]. Some thermosets exhibit yielding before fracture, an accurate description of their behaviour requiring the input of plasticity [2, 4]. On the other hand, thermoplastics exhibit a linear stress-strain response over a very short interval (under 1% deformation) and no clear yield point (the stress-strain curve gradually decreases its slope over a given strain interval) [1, 7, 8]. The stress-strain response of rubbers has a different shape (the characteristic 'S' curve) and can only be accurately modelled with the use of hyperelastic models, such as the Neo-Hookean formulation [9], Yeoh formulation [10], the Ogden formulation [11], the Arruda-Boyce formulation [12] or the implicit Marlow formulation [13]. These characteristics are presented in **Figure 1a**.

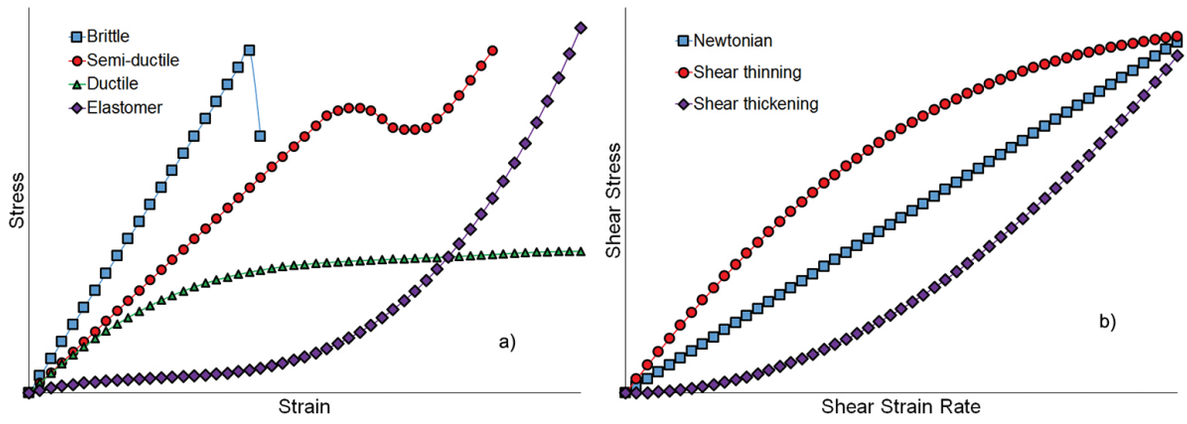

Figure 1. Mechanical behaviour of polymers: types of stress-strain response (a) and types of viscous flow (b).

Regarding the flow component, three models are usually employed to describe viscosity: the Newtonian fluid is the basic model in describing flow, where the shear stress increases linearly

http://dx.doi.org/10.5772/64563

with the shear strain rate (i.e. water). For other types of fluids, the viscosity increases exponentially with the increase in strain rate (i.e. honey, quicksand, oobleck). They are called shear-thickening fluids or dilatants. Fluids that exhibit a logarithmic increase in shear stress with shear strain rate are called shear-thinning fluids or pseudoplastic fluids (i.e. blood, paint, ketchup).

In modelling viscoelastic materials, a common approach is the use of mathematical models that incorporate both elastic and viscous elements. The aforementioned Maxwell and Kelvin models used two components, namely an elastic element (spring with an elastic modulus E) and a damping element (dashpot with a damping coefficient η), connected in series (Maxwell fluid, **Figure 2a**) or in parallel (Kelvin solid, **Figure 2b**). Note that the elastic element can undergo both normal and tangential loadings along all directions. More advanced models increase the number of elements in order to capture the behaviour of the viscoelastic material more accurately. Examples of such models are the three-parameter fluid, the four-parameter solid (**Figure 2c**), the generalized Maxwell fluid or the generalized Kelvin solid (models which imply the use of a number of Maxwell and Kelvin elements connected in parallel or in series, respectively) [5, 6].

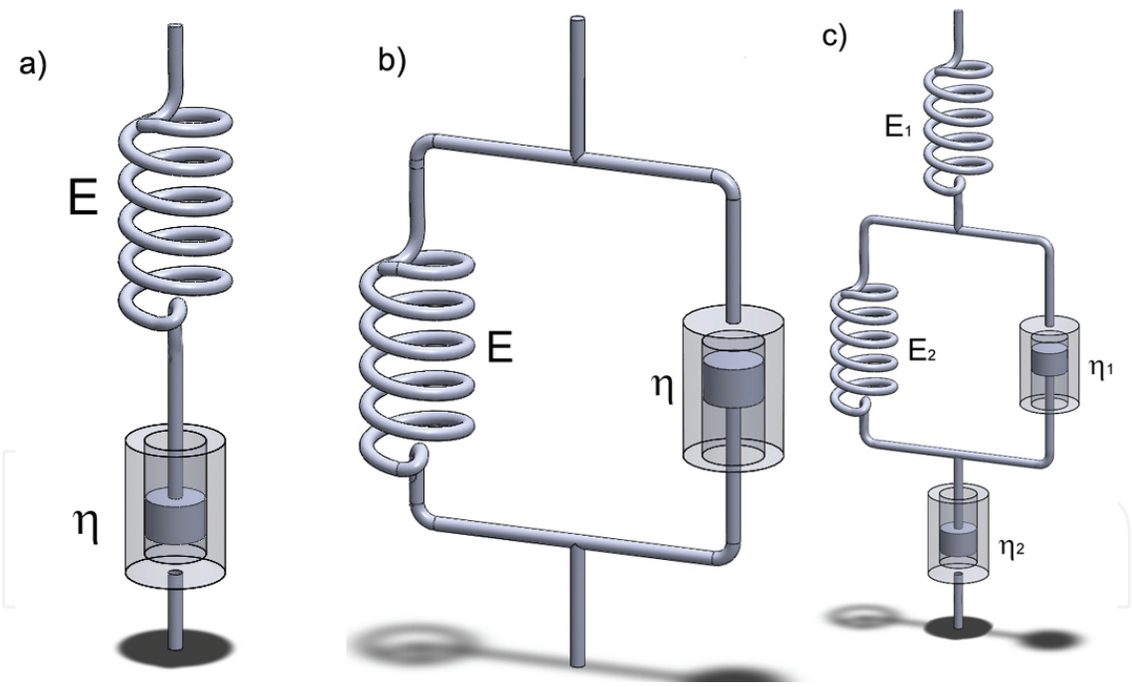

Figure 2. Mathematical models for the Maxwell fluid (a), Kelvin solid (b) and four-parameter solid (c).

For a higher degree of accuracy, the linear elastic response of the elastic element can be replaced with hyperelasticity, and the Newtonian fluid characteristic of the dashpot can be replaced with either a shear-thickening or a shear-thinning model. Viscoplasticity can be modelled by introducing a rate-independent flow component ('slip' element) in the presented mathematical models.

Other methods of modelling viscoplasticity consider a phenomenological approach. A notable example is the work of A.D. Drozdov and collaborators. Their constitutive models for various thermoplastics and elastomers consider the total deformation being composed of a sliding part and an elastic part and the stress-strain relation being governed by a strain-energy density function. The resulting constants and parameters are eventually fitted with the experimental data [14–16].

Considering the loading conditions, the same polymer can exhibit different behaviours: it can be characterized by either a glassy state (stiffer response, sometimes brittle) or a ductile state (a compliant response, yielding before fracture). The transition region between the two states is called the glass transition temperature (GTT) [3–6]. It is usually determined in temperature-sweep dynamic mechanical analysis (DMA) tests and can be extrapolated for strain rates using the time-temperature superposition.

One of the most notable examples of misestimating the mechanical properties of polymers is the case of the Challenger Space Shuttle disaster (28 January, 1986). The Presidential commission tasked with investigating the accident concluded that, due to the low temperatures recorded during the space shuttle launch, the rubber O-rings sealing the aft field joint, on the right solid rocket booster, became less resilient and ultimately failed. This allowed the pressurized hot gasses to make contact with the external tank, causing structural failure [17].

The investigated material of this study is a polyamide-based (PA) semi-crystalline thermoplastic polymer that was developed for low-temperature applications. Being established as the material used in manufacturing various components, it was observed that the given component's response to external loadings differed from the initial behaviour, after a certain period of service. Limited data were provided by the material supplier, so an extensive experimental plan was set up in order to determine the time and temperature dependency of the polyamide.

2. Experimental investigations

Considering the in-service conditions that the components manufactured from this compound are subjected to, an experimental plan was devised in order to capture the variation in mechanical properties with test parameters such as time (rate dependency and creep), temperature and humidity, as well as for several loading conditions (monotone and cyclic tests).

2.1. Monotone tests

2.1.1. Time dependency

The studied polyamide's variation of the mechanical properties with time was investigated for short-term (strain-rate-dependent tensile tests) and long-term scenarios (creep tests).

http://dx.doi.org/10.5772/64563

2.1.1.1. Strain-rate-dependency tests

Tensile tests represent the most facile experimental investigations used for the determination of mechanical properties of materials. With the evolution of universal testing machines over the past decades, materials of any class can be easily characterized in terms of their stress-strain behaviour, stiffness, strength and yield point.

For this study, strain-rate-dependent tests were performed on injected dumb-bell specimens, in accordance with ISO 527 [18]. The strain rates were chosen on a logarithmical scale, corresponding to the crosshead travel values suggested by the test standard: 0.00028, 0.0028, 0.028, 0.28 and 2.8 s^{-1} (corresponding for crosshead travel speeds ranging from 2 up to 20,000 mm/min).

Quasi-static tests were performed on two test systems: a ball-lead screw-driven electromechanical Zwick Z250 machine (for strain rates from 0.00028 up to 0.028 s^{-1}), equipped with a 10-kN load cell and on a servo-hydraulic Schenk PC63M (for a strain rate of 0.28 s^{-1}), equipped with a 40-kN load cell. In both cases, the strains were being recorded with an incremental extensometer on a gauge length of 50 mm.

The dynamic tests were performed on a servo-hydraulic Instron VHS 160/20 machine, equipped with a Kistler 9017A 400-kN piezoelectric load washer, mechanically preset at 200 kN. Strains were recorded through digital image correlation, using a high-speed camera at 190,000 frames per second, the images being processed using the ARAMIS system by GOM. Higher strain rates were also investigated but no clear results could be obtained due to system ringing, caused by the propagation of stress waves through the testing equipment [8, 19, 20].

The stress-strain curves for the strain-rate-dependent tests are presented in **Figure 3** [8]. The variation in elastic modulus and tensile strength with strain rate is presented in **Figure 4**. The elastic modulus was calculated using the recommendations from ISO 527 [18].

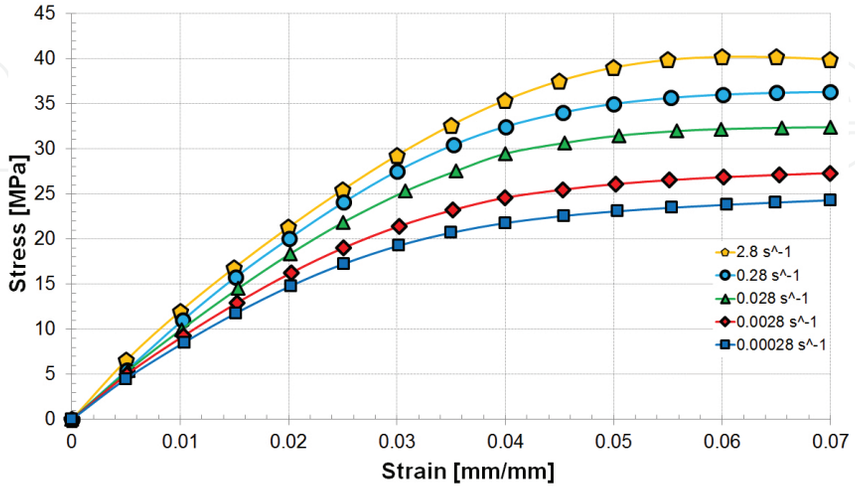

Figure 3. Stress-strain curves for strain-rate-dependency tests.

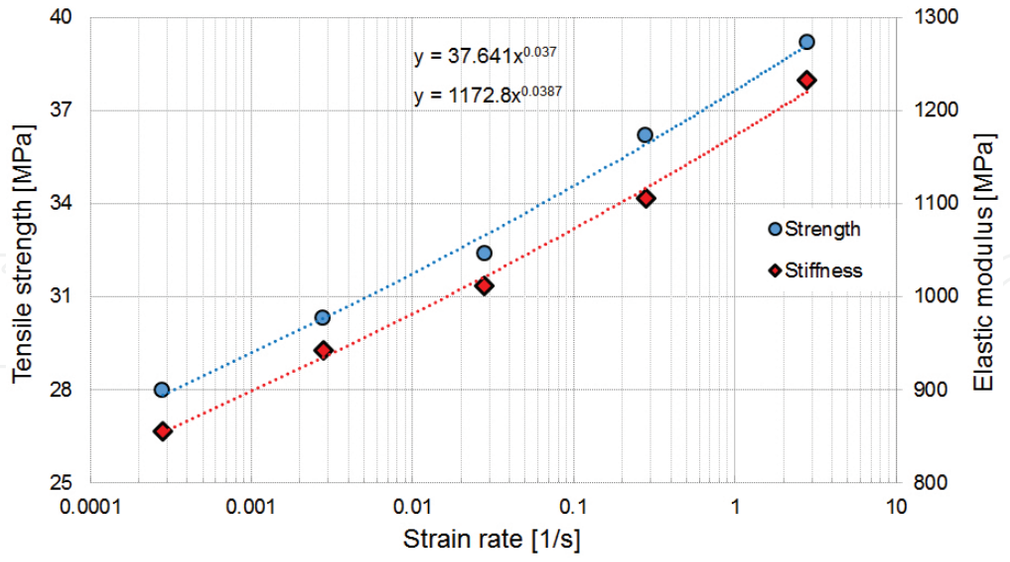

Figure 4. Variation of elastic modulus and tensile strength with strain rate.

Figure 4 shows that a correlation between the increase in tensile strength and stiffness with strain rate can be observed, both trend lines having similar exponents.

Regarding the stress-strain behaviour, **Figure 3** shows that the yield strain decreases with an increase in strain rate. Tests performed at low speeds, when the viscous effects become more significant, determine no clear yield point. By analysing the shape of the stress-strain curves, it can be observed that the linear region is very small, almost unnoticeable. An analysis of the variation of stiffness with strain, for the investigated strain rates, is presented in **Figure 5**.

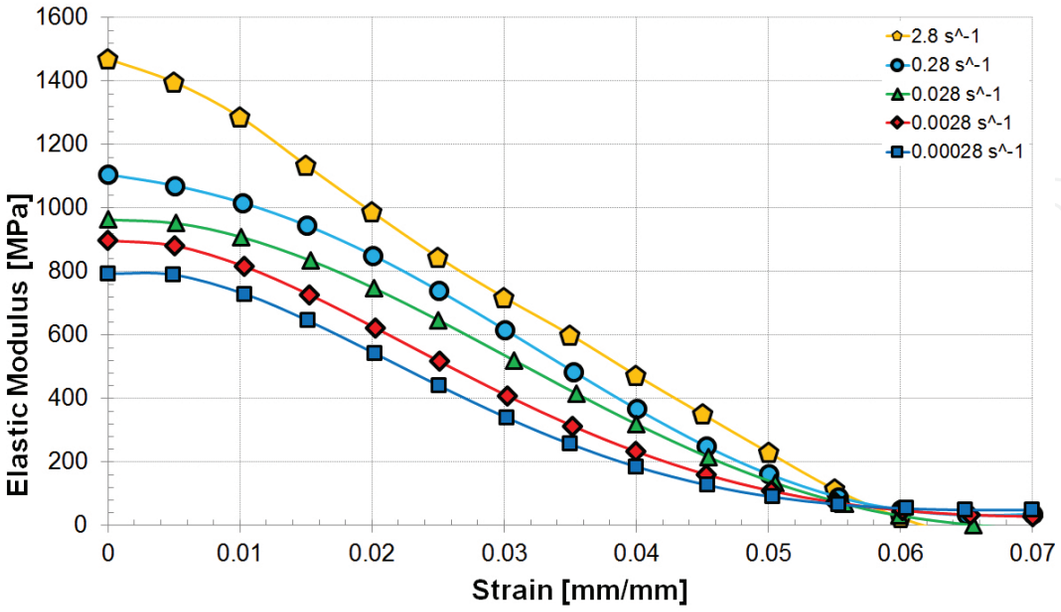

Figure 5. Variation of stiffness with strain, for the investigated strain rates.

http://dx.doi.org/10.5772/64563

2.1.1.2. Creep tests

Creep tests investigated the long-term influence of time on the mechanical properties of the polyamide, and were performed on a 5-kN Zwick/Roel machine. Three loading levels were used, corresponding to 30, 60 and 90% of the estimated yield stress [21], maintained for a period of 24 h. The normalized compliance is calculated with Eq. (1), test result being presented in **Figure 6**.

$$d(t) = \frac{D(t)}{D(0)} = \frac{\varepsilon(t)}{\sigma(0)} \cdot \frac{\sigma(0)}{\varepsilon(0)} = \frac{\varepsilon(t)}{\varepsilon(0)} \tag{1}$$

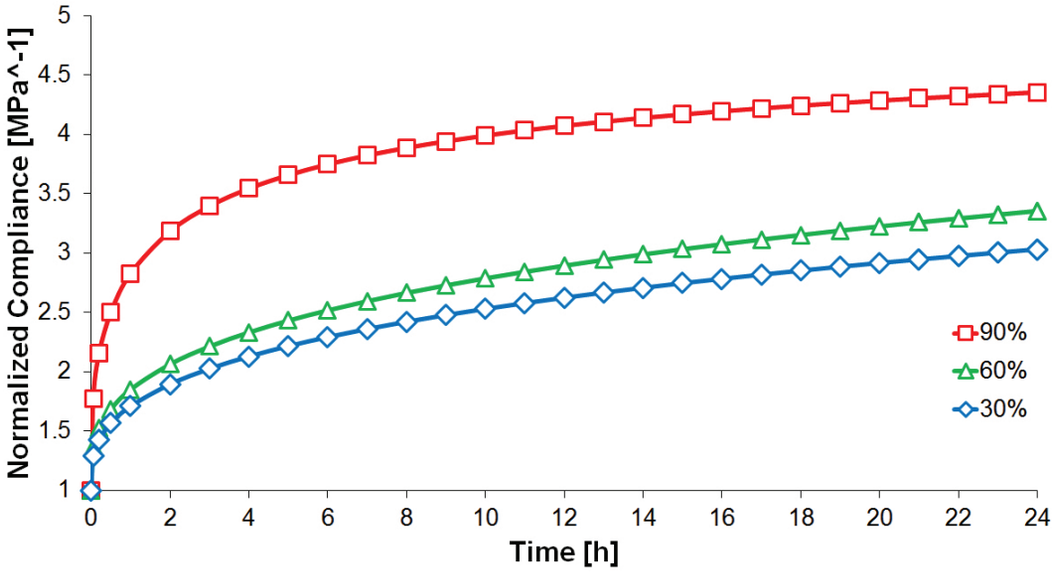

Figure 6. Creep tests at 30, 60 and 90% tensile strength.

A drastic increase in tensile compliance can be observed in the first hour of each test, after which the increase becomes gradually smaller. Given the non-linear behaviour of the material, the values for compliances differ for each level of loading, higher loads determining higher compliances.

Comparing the variation of the normalized tensile compliance with time, between the tests performed at high deformations (90% of the yield stress) and low deformations (60 and 30% of the yield strain), a significant difference is noticed. Although increased stress levels determine higher compliances, there is no linear correlation between the variations of the two parameters, but rather an exponential one. The observed phenomenon is caused by strain softening of the material. As the total strain grows towards the yield point, the role of the viscous and plastic components becomes significant. Given the fact that no clear plateau was recorded, one can conclude that the viscous strain did not reach saturation after 24 h of constant loading.

2.1.2. Temperature-dependency tests

The tests were performed with a crosshead travel speed of 20 mm/min on a ball-lead screw-driven electromechanical Zwick Z250 machine equipped with an environmental chamber. Strains were recorded with an incremental extensometer. The stress-strain curves are presented in **Figure 7** and the variation of tensile strength and elastic modulus with temperature is presented in **Figure 8**.

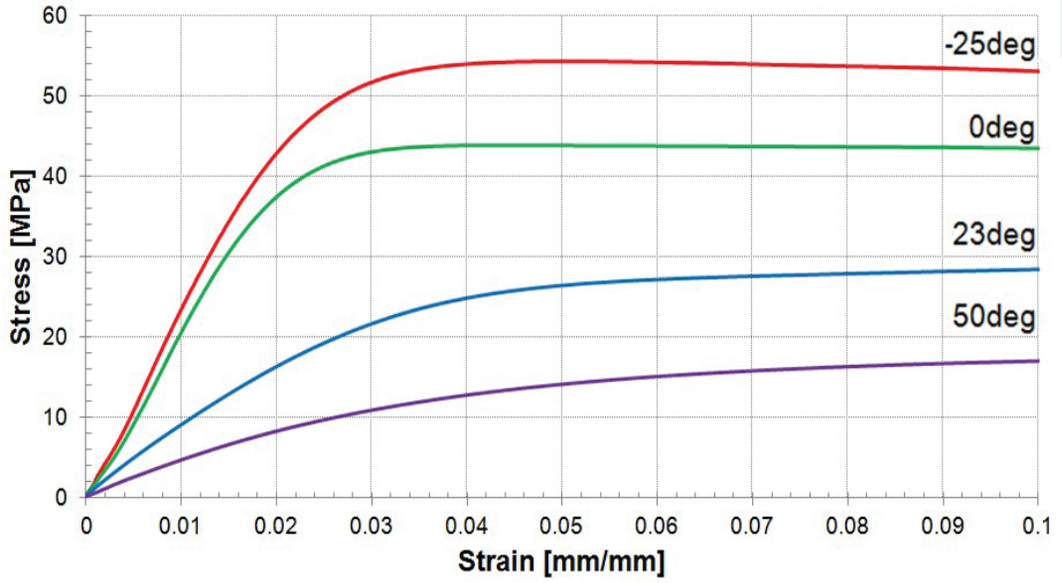

Figure 7. Stress-strain curves for temperature-dependency tests.

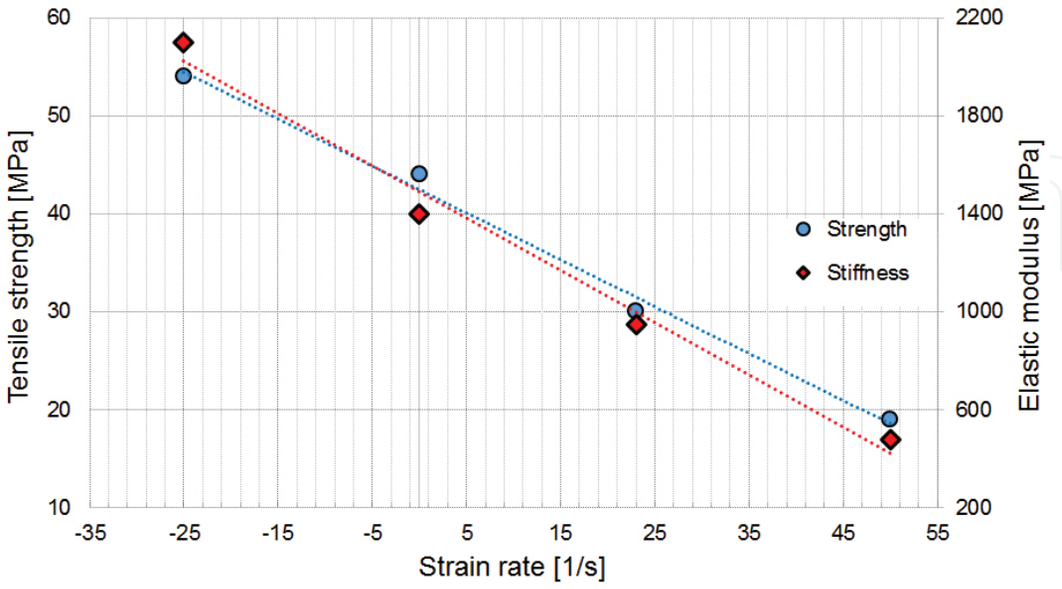

Figure 8. Variation of elastic modulus and tensile strength with temperature.

http://dx.doi.org/10.5772/64563

The same type of non-linearity as with strain-rate-dependent tests is observed; the instantaneous elastic modulus does not remain constant and varies with strain (**Figure 9**). For the low-temperatures tests, a toe region can be observed: the maximum elastic modulus does not coincide with the initial value, which occurs around 0.007-mm/mm deformation. After an abrupt decrease, the instantaneous modulus reaches values close to 0, for the plateau region (around 0.035 mm/mm strain). For higher temperatures, the variation is characterized by a uniform descent until the yield point, similar to ambient temperature tests.

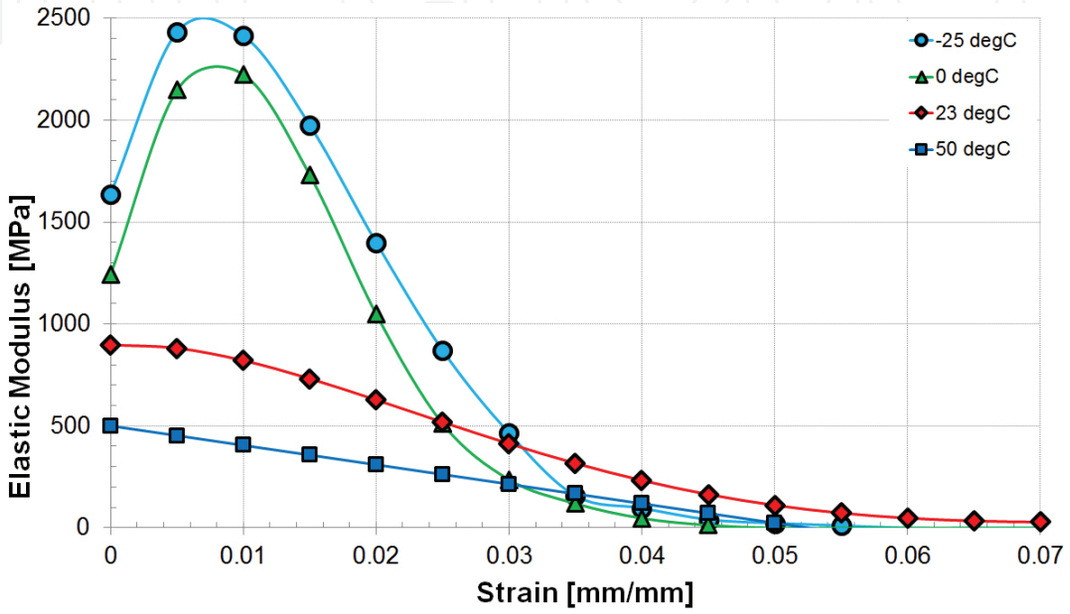

Figure 9. Variation of stiffness with strain for the investigated temperatures.

2.2. Cyclic tests

A more comprehensive look at the viscoplastic properties of the studied polyamide was obtained by performing cyclic tests, namely DMA tests, Mullins' effect tests and low-cycle fatigue (LCF) tests.

2.2.1. DMA tests

In this study, two types of DMA tests were performed. First tests consisted of temperature-sweep low-strain investigations (~0.1% strain), performed in single cantilever on a 'conventional' TA Instruments Q800 DMA machine. The second tests consisted of large-strain DMA tests (1.5–4.5% deformation), performed in tension on an electromagnetic Instron Electropuls machine.

The temperature sweep tests determined a glass transition temperature of 38.5°C at 1 Hz (**Figure 10**) and of 41.2°C at 10 Hz, which explains the large variation in stiffness and strength observed during the temperature-dependency tensile tests.

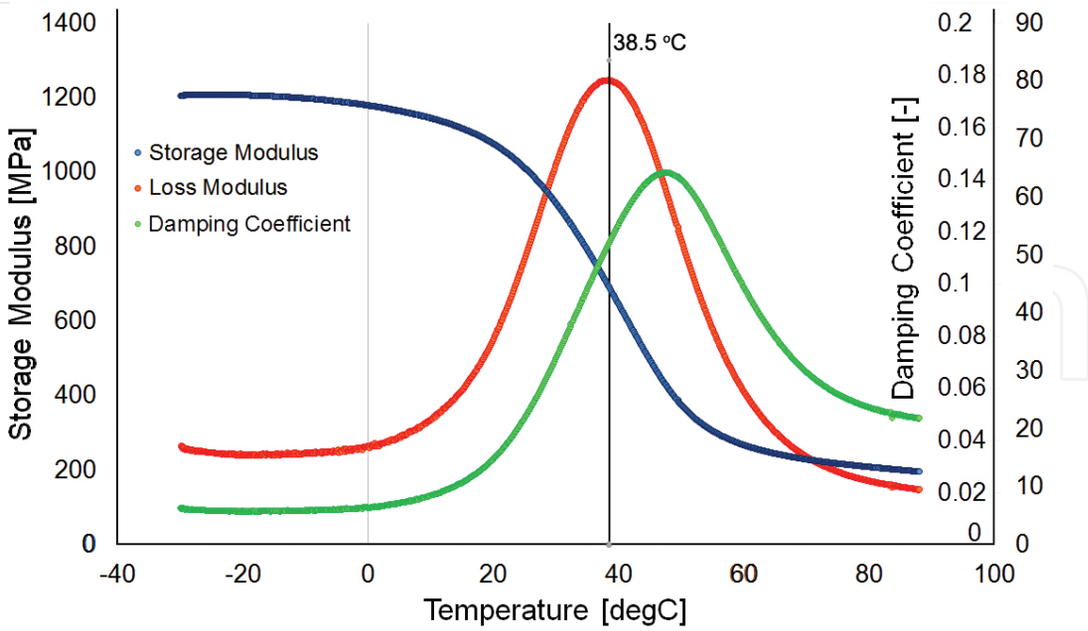

Figure 10. DMA results for a temperature sweep test performed at 1 Hz in single cantilever.

Considering that usual component undergoes higher deformations during service and that the instantaneous elastic modulus varies with strain (**Figure 5**), large-strain DMA tests were carried out in order to record the variation of the dynamic moduli with frequency and with amplitude.

For all the investigated frequencies and amplitudes, a similar trend was observed: the storage modulus increased while the damping coefficient and the loss modulus decreased with frequency (**Figure 11a**). When investigating the moduli variation with amplitude, it can be noted that the elastic potential decreases with amplitude. The loss modulus and damping coefficient increase with the amplitude until it reaches values of around 1.6 mm (equivalent of 4.3% total strain), when, due to the contribution of the remnant strain (plastic and viscous strains), the two parameters plateau (**Figure 11b**).

2.2.2. Mullins' effect tests

The cyclic-induced-softening behaviour of polyamides is determined by various deformation mechanisms that can occur. In literature, the non-recovered deformation observed when the loading stops is usually referred to as 'plastic strain' or 'permanent strain' [4, 5]. However, due to the viscous effects caused by the polyamide's structure, a part of that remnant deformation is recovered through relaxation (the stored potential energy causes some macromolecules to regain their initial position). The irreversible part of the deformation is caused by the slippage of the atomic planes in the crystalline phase (similar to metal plasticity [22, 23]) or by macromolecular chain scission [1].

In consequence, the semi-crystalline structure of the polyamide causes a specific behaviour during deformation, the strain being divided into three categories: instantaneous elasticity

http://dx.doi.org/10.5772/64563

(recovered immediately after the loadings stop), delayed elasticity (recovered after a certain time) and permanent deformation (caused by the irreversible change in structure). If the material is subjected to a constant load below the yield stress, the main deformation component that will be observed is the instantaneous elastic strain. If the loading is maintained for a longer time (creep tests), an increase in the total deformation is observed, due to the accumulation of viscous strain. If the specimen is strained towards yielding and beyond, the permanent deformation starts to become significant while the reversible strain begins to plateau [2, 7].

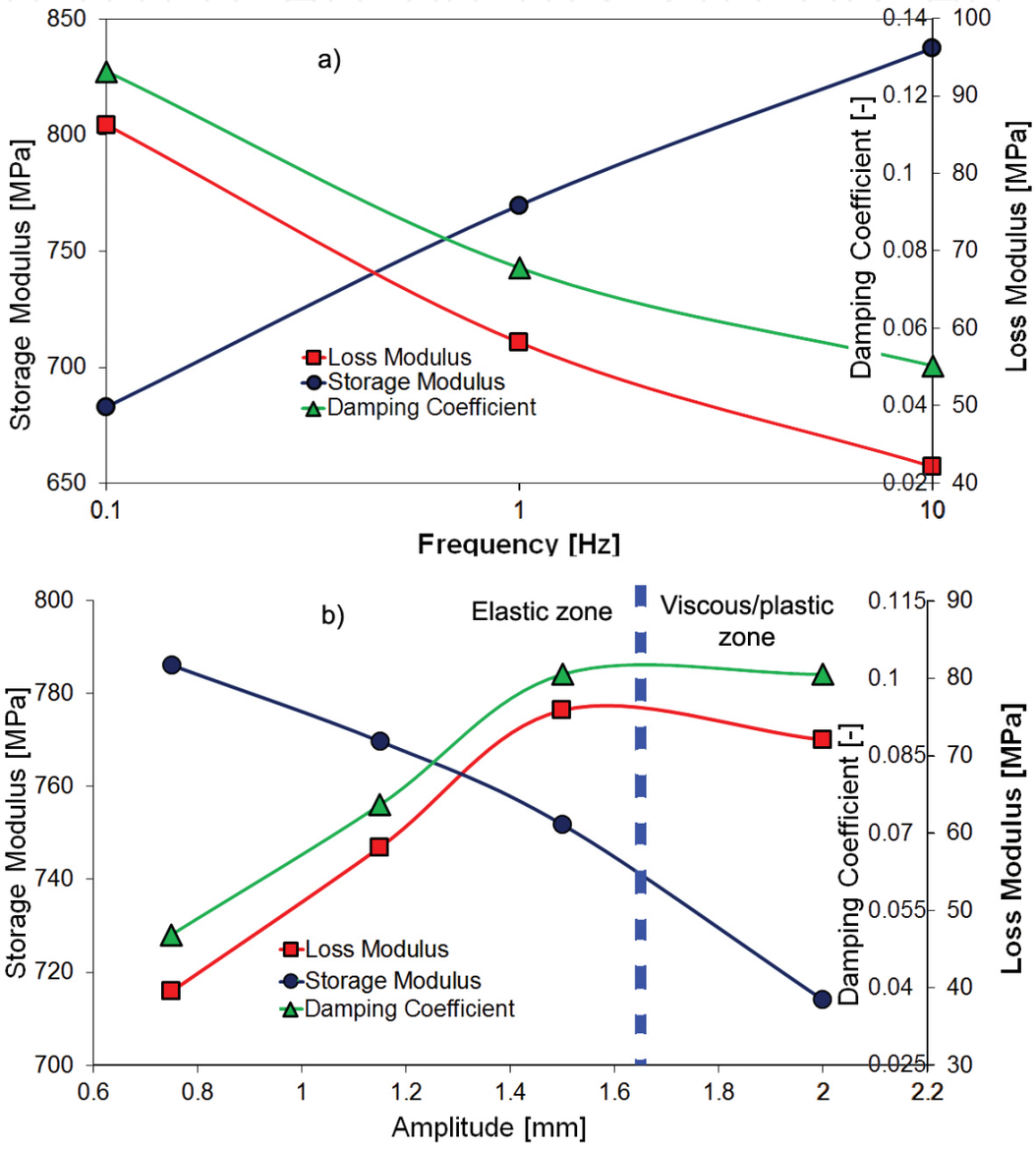

Figure 11. Results for DMA tests performed at high strains for frequency variation (a) and amplitude variation (b).

The same scenario is observed for cyclic loadings. **Figure 12** presents the strain decomposition for a sine loading. The total strain ε^{tot} is the sum of the instantaneous elastic strain ε^{el}, the viscous strain ε^{vsc} and the plastic strain ε^{pl}. In this example, the cyclic loadings are performed in strain

control, thus ε^{tot} presents a constant sine variation in each cycle. The plastic strain ε^{pl} reaches a maximal value with the peak of the cycle while the viscous strain ε^{vsc} presents a steady increase until it reaches saturation (this point being considered the steady-state behaviour in cyclic loadings). The instantaneous elastic strain ε^{el} is obtained by subtracting ε^{pl} and ε^{vsc} from ε^{tot}.

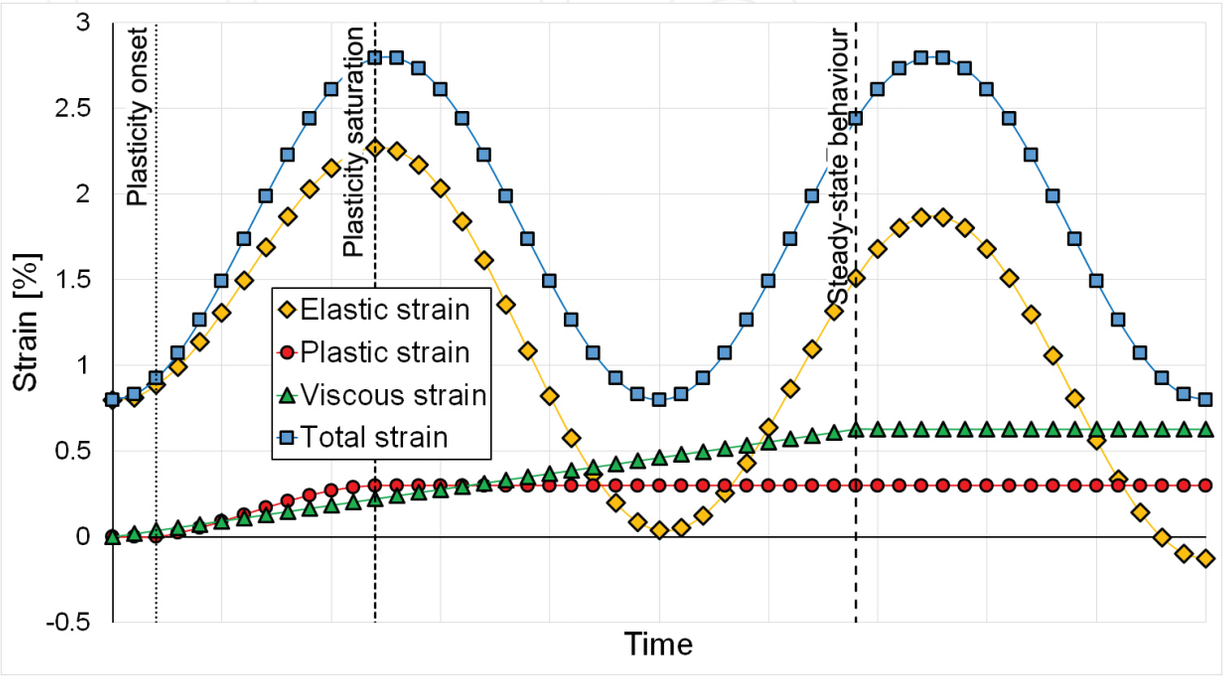

Figure 12. Strain decomposition for a tensile cyclic test on a viscoelastic material.

Mullins' effect tests were initially developed for rubber testing but were implemented for other types of polymers such as thermoplastic elastomers and semi-crystalline thermoplastic polymers [24–26]. Three main material characteristics are distinguishable for such tests: hysteresis of energy, strain softening and strain hardening [27–29].

The graphic representation depicting the first loading/unloading cycle of each amplitude is called the primary hyperelastic behaviour; the material's loading path exhibits strain hardening when loaded to stress values higher than the current cycle. If the material is subjected to several cycles with the same amplitude, it exhibits a strain-softening phenomenon, caused by the accumulation of viscous strain, as described above. After a certain number of cycles of the same amplitude, the behaviour stabilizes to a stress-strain curve of the same shape, due to the saturation of viscous strain, called the permanent set [30, 31].

The first set of Mullins' effect tests was performed on a 10-kN Walter + Bai servo-hydraulic fatigue machine. The experimental programme consisted of three blocks of different amplitudes with 10 cycles being performed in each block (**Figure 13a**). The machine was set in displacement control, with an equivalent crosshead travel of 25, 50 and 75% of the approximated yield stress. The test speed was held constant at 2 mm/min, results being presented in **Figure 13b** [31].

http://dx.doi.org/10.5772/64563

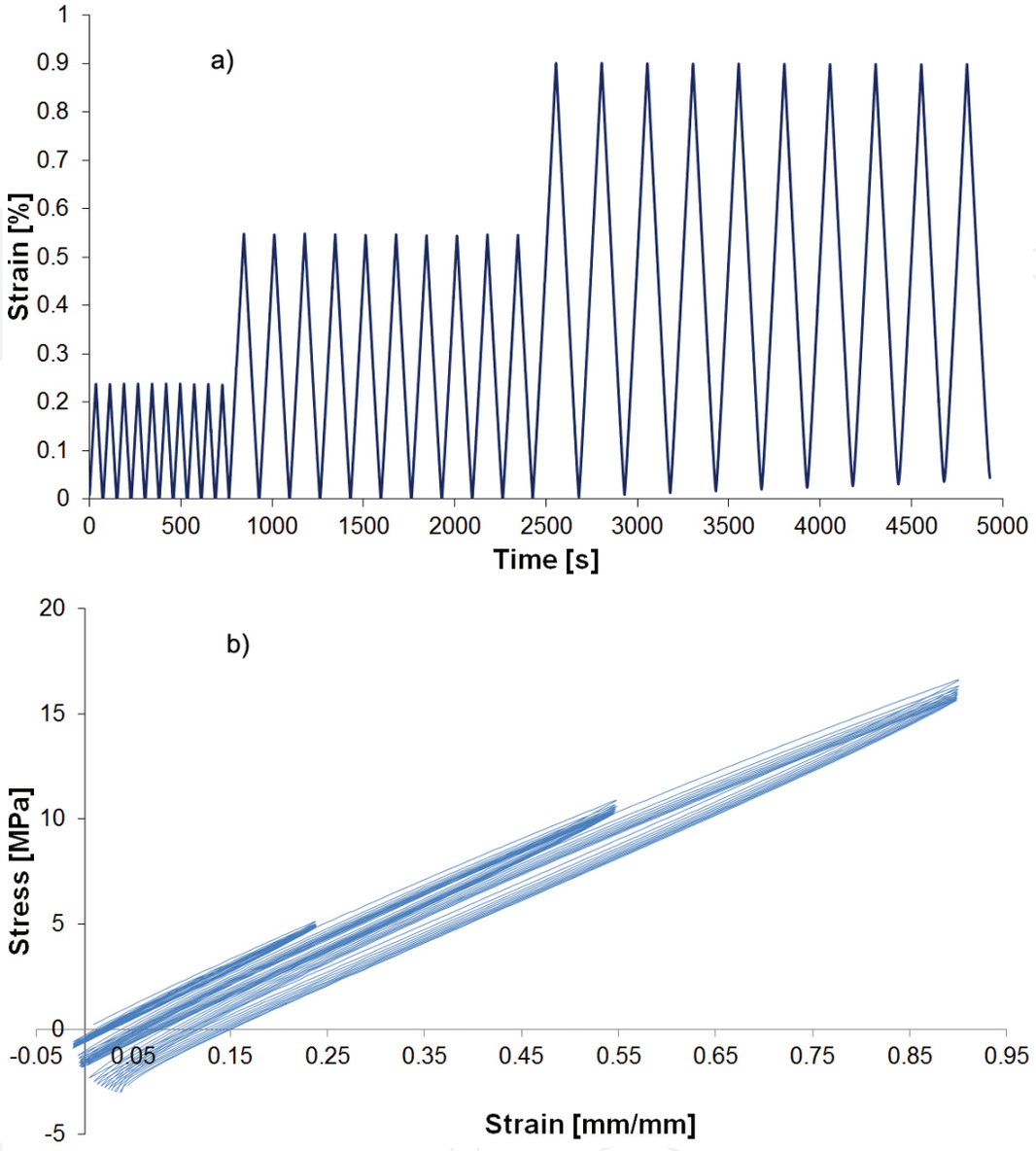

Figure 13. Program set-up (a) and experimental results (b) for the Mullins' effect test.

Considering the results presented in **Figure 13**, for Mullins' effect tests performed below the yield point, the investigated polyamide exhibits energy dissipation (hysteresis) and strain softening. In order to gain insight about the strain hardening, cyclic tests that strain the material beyond the yield point had to be performed. Two such cyclic test protocols were designed, one having equal stress increments while the other having equal strain increments.

Mullins' effect tests with equal stress increment were performed on a Zwick Z250 machine that was programmed in stress control, strains being recorded with an incremental extensometer. The cyclic programme is presented in **Figure 14a**, and the test results are presented in **Figure 14b**. Having more cycles before the yield region, these tests gave insight about the strain decomposition in the elastic domain.

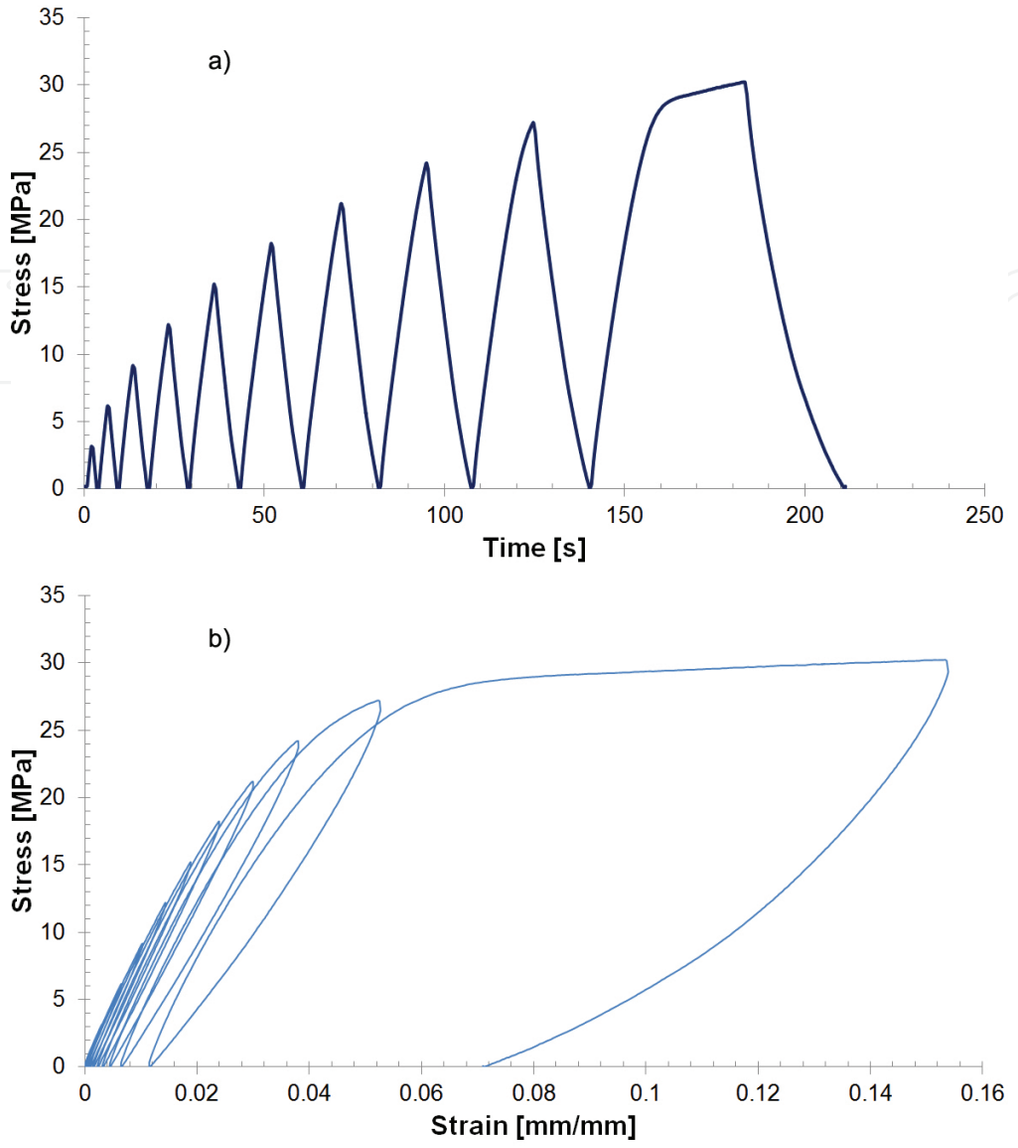

Figure 14. Program set-up (a) and experimental results (b) for the Mullins' effect test with equal stress increment.

Mullins' effect tests with equal strain increment were performed on the same Zwick Z250 machine, the machine being programmed in strain control. The test protocol is presented in **Figure 15a**, and the results are presented in **Figure 15b**. The strains programmed in these experiments went beyond the yield region, showing the material behaviour in the plastic domain. Considering the strain decomposition using cyclic tests, even though the tests deformed the specimens well into the plastic region, the elastic strain did not reach a plateau and kept increasing at a decelerated rate due to the delayed elasticity (**Figure 16**). These viscous effects can be noticed when unloading to zero stress, the material being relaxed and some of the energy consumed in deforming the specimen got recovered (the non-linear unloading path). It was also noticed that, similar to rubbers and elastomers, the studied polyamide exhibits strain hardening as well (the stress-strain response of the specimen tested in cyclic loadings resumes the path described by a virgin specimen, **Figure 17**).

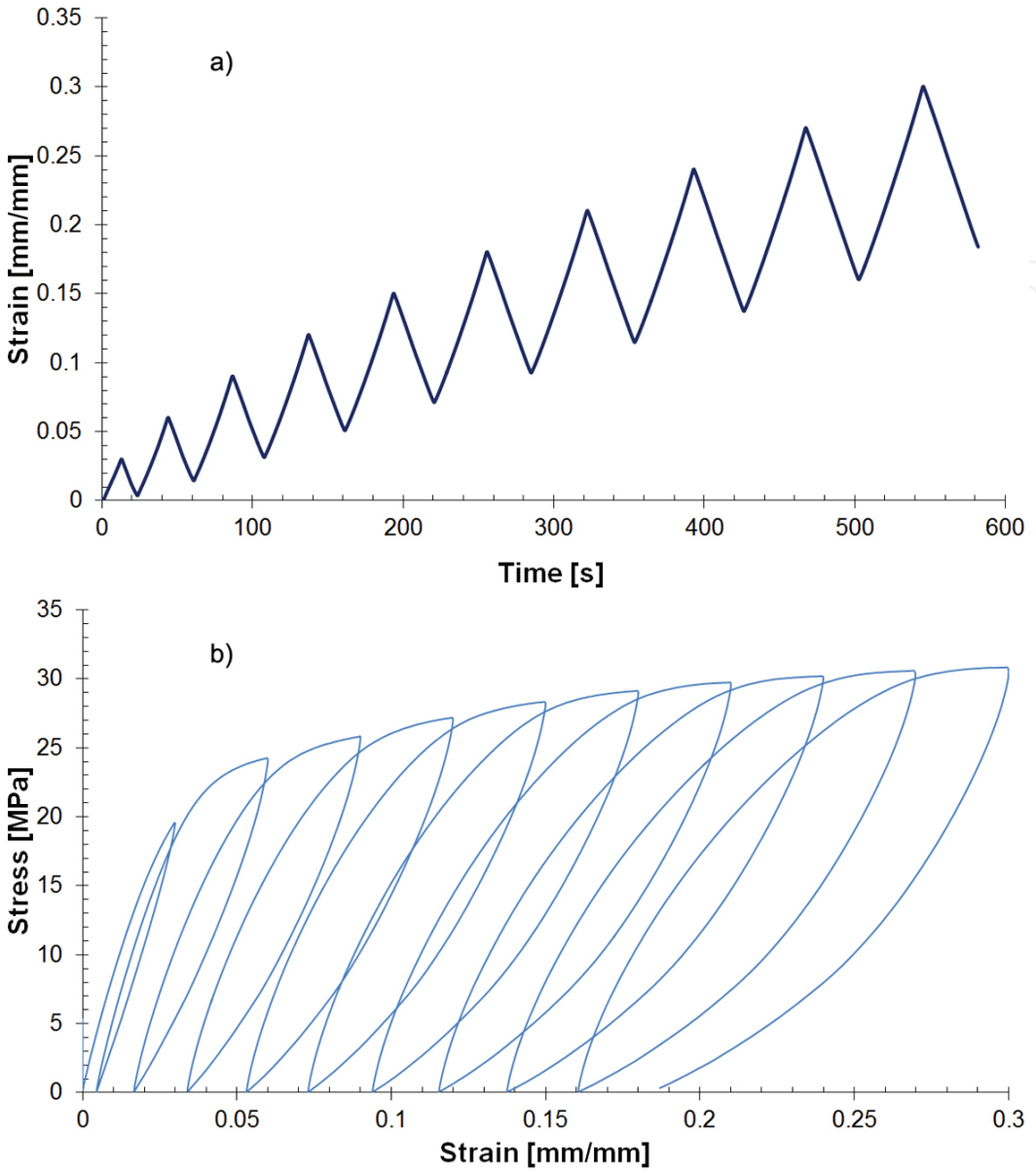

Figure 15. Program set-up (a) and experimental results (b) for the Mullins' effect test with equal stress increment.

2.2.3. Low-cycle fatigue tests

A better insight into the behaviour of the investigated polyamide in cyclic loadings was given through low-cycle fatigue tests. The experiments were performed in tension and strain control, with an *R*-ratio of 0.1. A 40-kN Schenk PC63M machine was used and was equipped with an environmental chamber, set at 23°C (to negate the effects of temperature variation) and the strains were recorded with a strain-gauge extensometer.

The influence of three parameters on the fatigue behaviour of the material was investigated: number of cycles, frequency and strain level (each parameter was varied in three steps). The test protocol also implied the investigation of the material recovery and permanent damage,

tensile tests being performed on fatigued specimens immediately after tests as well as after a recovery time of 24 h.

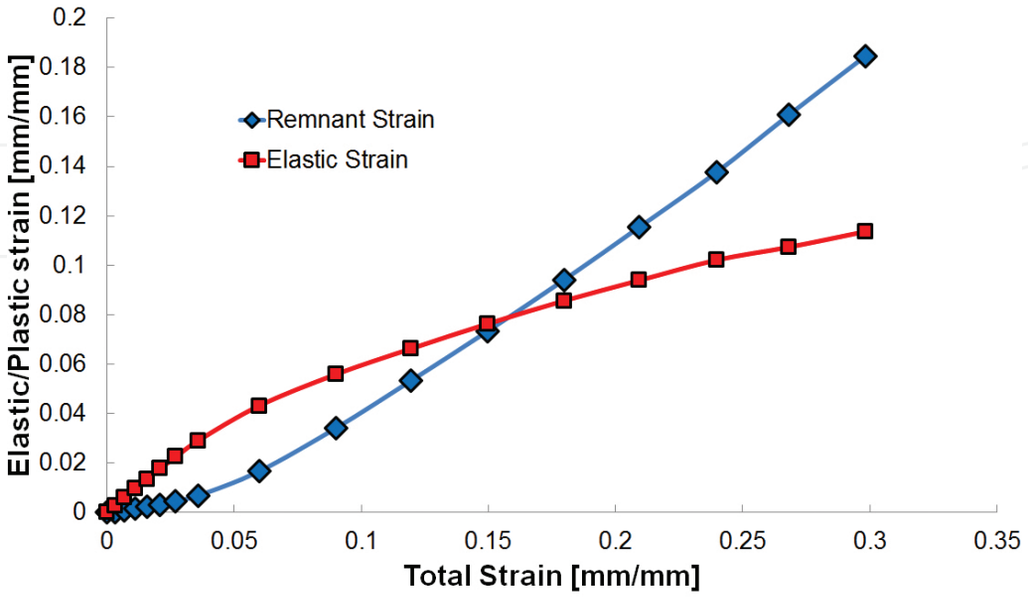

Figure 16. Strain decomposition using Mullins' effect tests.

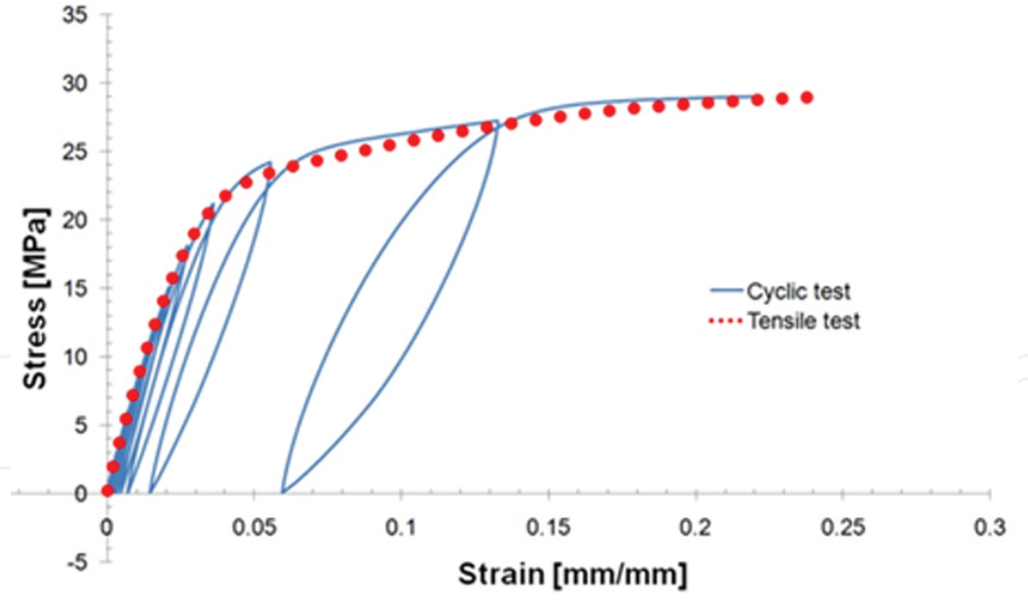

Figure 17. Strain hardening of the PA compound during cyclic loadings.

2.2.3.1. Effect of the number of cycles

Previous cyclic tests at constant amplitude performed below the yield point of the investigated material showed that remnant deformation is accumulated with each cycle, having a loga-

http://dx.doi.org/10.5772/64563

rithmic increase (due to the accumulation of viscous strain, as discussed above). This study aimed to determine after how many loading cycles the polyamide's viscous strain reaches saturation. Three values for the number of cycles were chosen: 5000 cycles (a), 10,000 cycles (b) and 50,000 (c). Each test was divided in five equal steps (blocks of 1000 cycles for (a), 2000 cycles for (b) and 10,000 cycles for (c)), the stress-strain response being recorded after each step. The frequency (5 Hz) and amplitude (0.0075 mm/mm with a pre-strain of 0.025 mm/mm) were maintained constant. **Figure 18** presents the variation in normalized tensile strength (peak stress value recorded after each loading block, divided by the initial value) with the number of cycles.

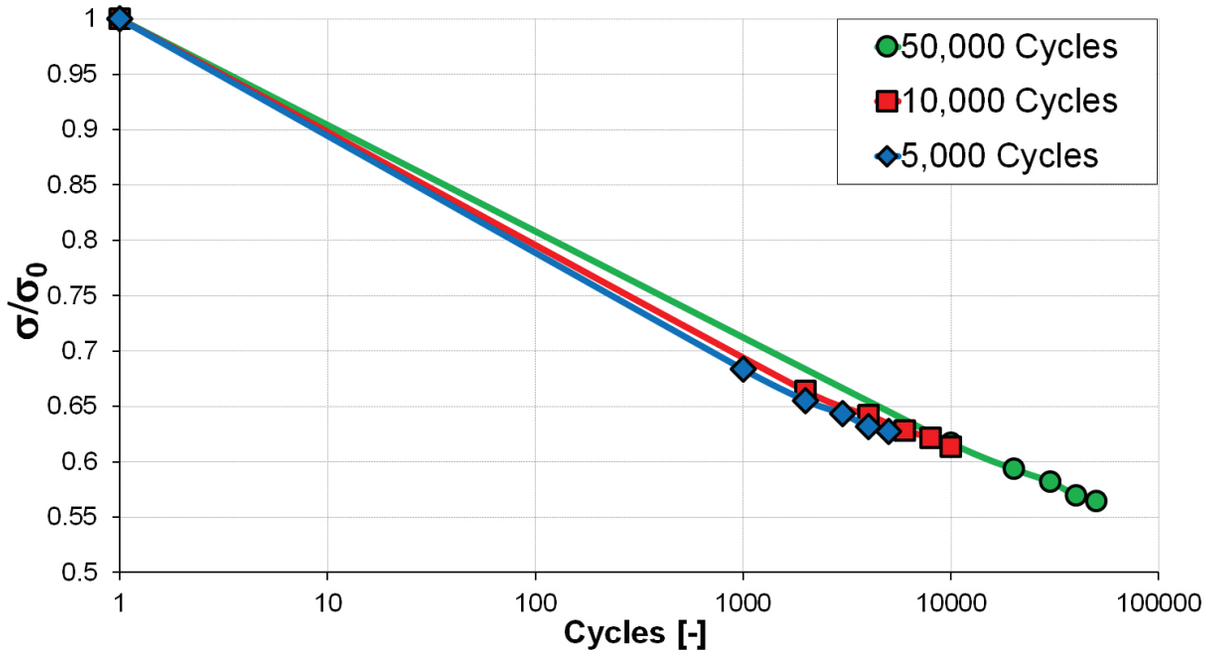

Figure 18. Variation of the normalized stress with the number of cycles.

As with the Mullins' effect tests, the LCF results show a considerable decrease in tensile strength in the beginning of the tests, followed by a steadier decrease as the number of cycles grew, the tensile stress number of cycle curves showing a linear variation on the semi-logarithmical scale.

The results of the tensile tests are presented in **Figure 19**. The behaviour of three specimens was plotted: a specimen subjected to LCF, tested immediately after the tests (denoted 'Instant'), a specimen rested for 24 h after it was subjected to LCF (denoted 'Recovery') and that of a virgin specimen (denoted 'Initial'). A negligible variation in the stress-strain response is observed, consisting of a lower stiffness up to 0.04-mm/mm deformation for the fatigued specimens tested immediately after LCF [32].

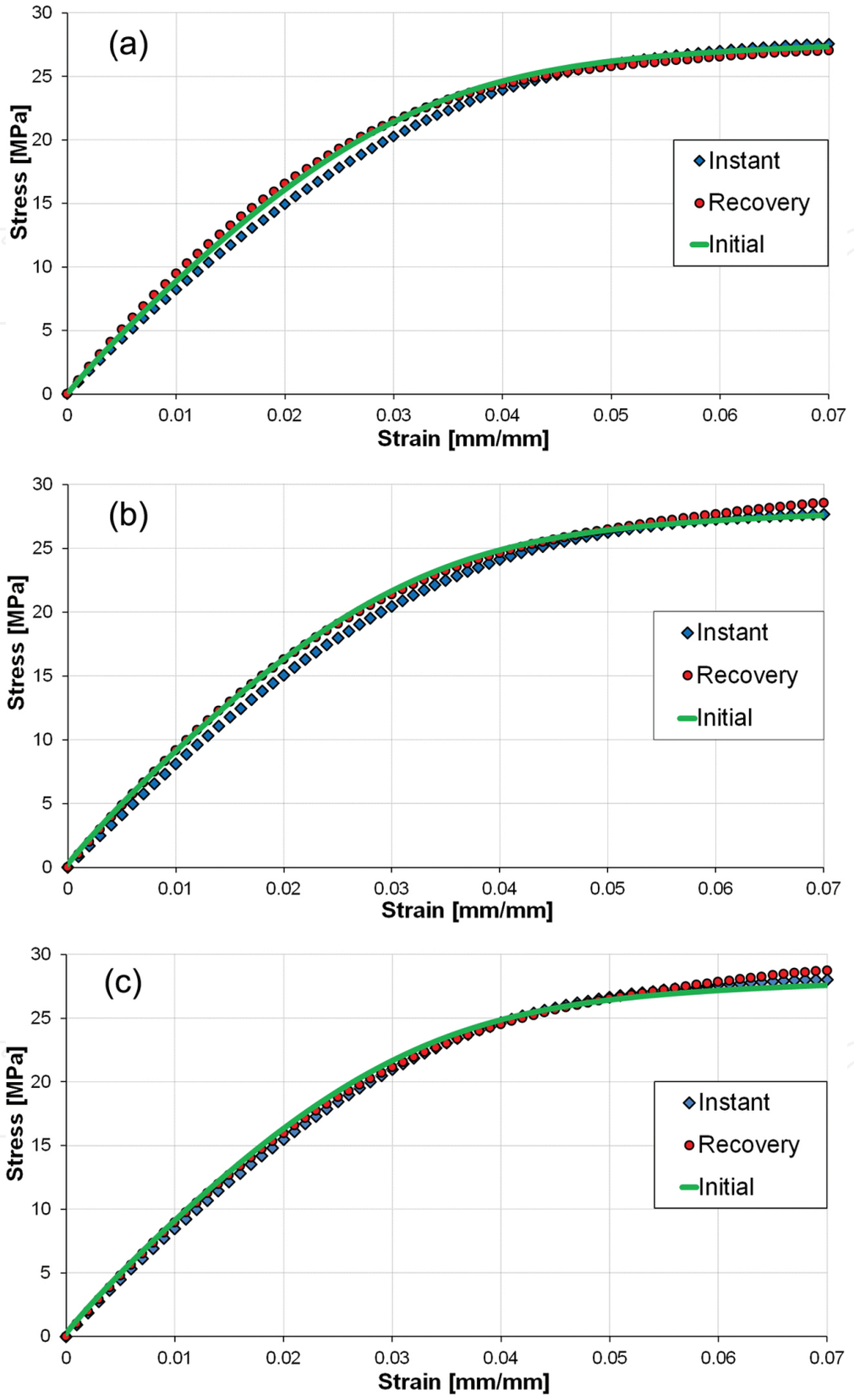

Figure 19. Tensile test comparison for (a) 5000 cycles, (b) 10,000 cycles and (c) 50,000 cycles.

http://dx.doi.org/10.5772/64563

2.2.3.2. Effect of frequency

The effect of strain rate on the mechanical behaviour of the studied polyamide in LCF was studied by the mean of frequency variation. Three values were chosen for this study: 3, 5 and 7 Hz. The strain levels were maintained constant and identical with the previous programme (0.025-mm/mm reference with 0.0075-mm/mm amplitude) and the total number of cycles was 5000. The results for the variation in normalized tensile strength of the cycles with the number of cycles for the three chosen frequencies are presented in **Figure 20**.

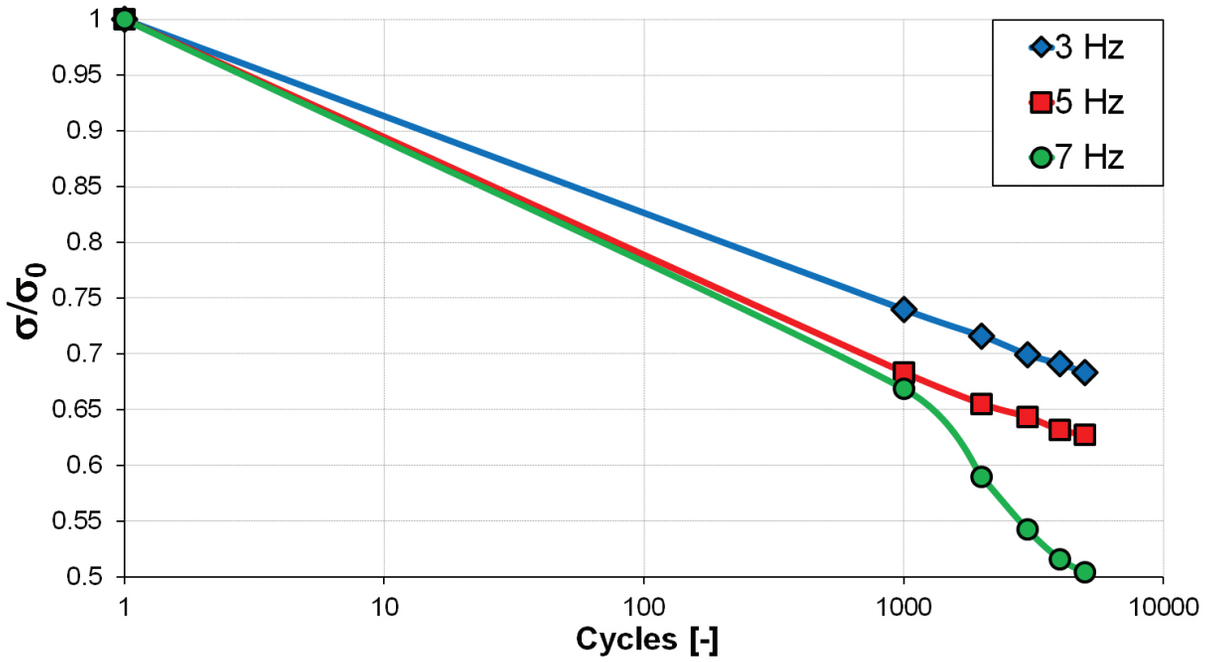

Figure 20. Normalized stress variation with the number of cycles for three different frequencies.

As with previous tests, higher strain rates determine higher reactions. Considering the normalized values, frequency affects the fatigue behaviour of the material: a linear behaviour (on the semi-logarithmic scale) is observed for lower strain rates (3 and 5 Hz), the apparent softening being proportionate with frequency. For the tests performed at 7 Hz, the normalized strength number of cycles behaviour is non-linear in the semi-logarithmic scale as the decrease in strength is more accentuated as the cycle count increases. This is due to the same mechanism responsible for shifting of the yield region observed in strain-rate and temperature-dependency tests (**Figures 3** and **7**): the viscous flow is being hindered and the effects of plasticity are more pronounced.

Tensile tests performed on previously untested specimens, specimens tested immediately after LCF tests and specimens tested 24 h after LCF tests show similar features as the results for the effect of number of cycles in terms of elasticity, but showing higher strengths at 0.07-mm/mm deformation. Results are presented in **Figure 21** [32].

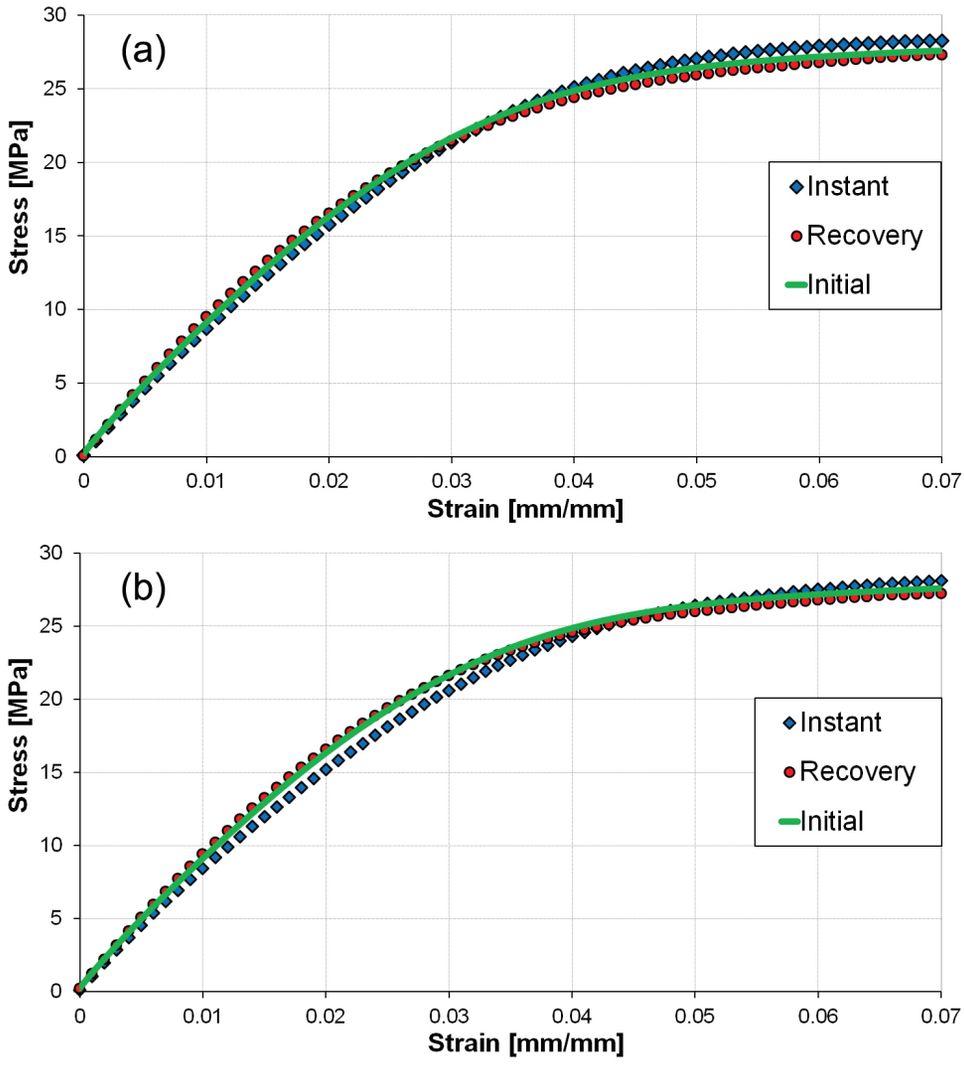

Figure 21. Tensile test comparison: 3 (a) and 7 Hz (b).

2.2.3.3. Effect of strain

As seen with previous tests and depicted in **Figure 12**, the remnant deformation accumulates with the increase in strain. The effect of the straining level in cyclic loadings on the fatigue behaviour of the polyamide was investigated by choosing three pre-strains (0.025, 0.035 and 0.045 mm/mm) and maintaining the same amplitude (0.0075 mm/mm), same frequency (5 Hz) and the same number of cycles (5000). The variation of the normalized strength with the number of cycles is presented in **Figure 22**.

The tensile test results performed on the same three types of specimens are presented in **Figure 23**, showing a slight lower response between 0.01- and 0.05-mm/mm deformation [32].

Figure 22 shows that the reference strain level has a small influence on the normalized stress variation with the number of cycles, showing linear variation on the semi-logarithmic scale and lower values of the normalized stress for higher strains. **Figure 24** explains this phenom-

http://dx.doi.org/10.5772/64563

enon: as the material is strained to higher values, its remnant deformation increases. At a reference strain of 0.025 mm/mm (denoted with a vertical red line in **Figure 24**), the remnant strain values are around 0.007 mm/mm. At 0.045-mm/mm reference strain (vertical red line in **Figure 24**), the remnant strains reach values of 0.018 mm/mm. The higher remnant strains accumulate and determine a drop in the tensile strength of each cycle.

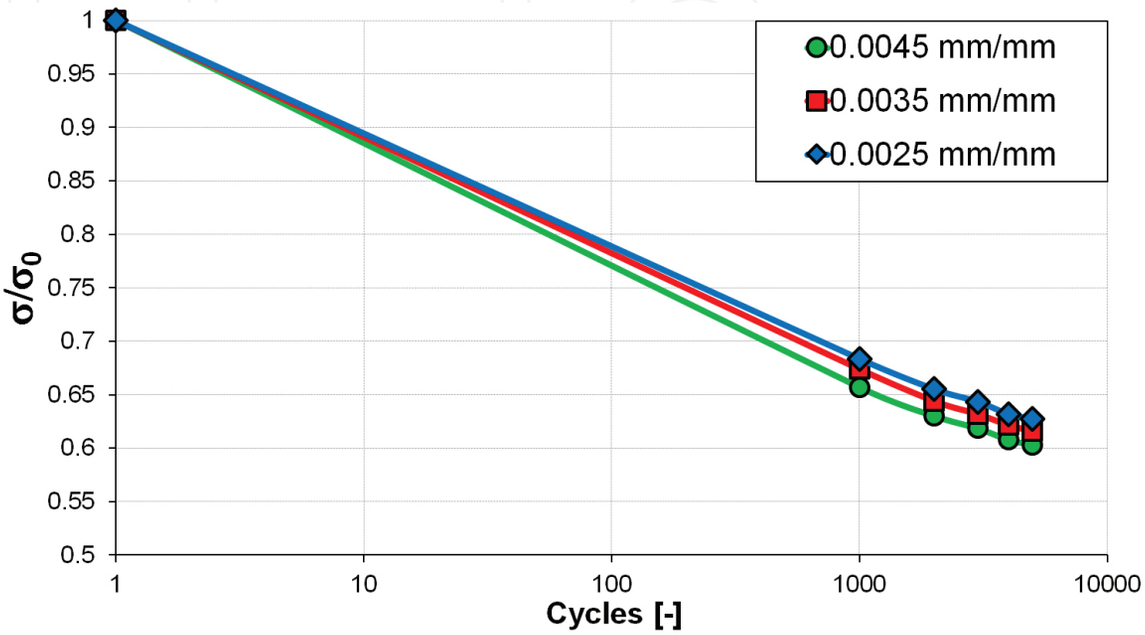

Figure 22. Normalized stress variation with reference strain.

In order to acquire a more in-depth analysis of the LCF behaviour, a study of the energy dissipation was performed, analysing specific stress-strain cycles taken from each recording step, from all tests. The dissipated energy in each cycle was evaluated by calculating the area enclosed by the hysteresis described by the loading-unloading stress-strain curve.

For the tests that investigated the influence of the number of cycles, it was observed that the dissipated energy decreases linearly on the semi-logarithmic graph (**Figure 25a**) until 10,000 cycles, after which the steep of the curve decreases.

A different trend was observed in the case of frequency-influence tests. Experiments performed at 3 and 5 Hz show a linear decrease in dissipated energy with the number of cycles while those performed at 7 Hz show an increase (**Figure 25b**). This is caused by the viscous characteristic of the material. At lower strain rates, viscous flow is more pronounced (as the macromolecules have the time to slip past each other [1, 5, 6]) and more energy is dissipated through slip (for the tests performed at 3 Hz, the values for the dissipated energy are almost triple in comparison to the tests at 5 Hz). At higher strain rates, the material 'freezes' and less energy is dissipated in the beginning of the tests. As the number of cycles grows, at low strain rates, viscous strain reaches saturation (a decrease in dissipated energy) while remnant strain accumulates at high strain rates (due to plastic strain accumulation), hence an increase in dissipated energy.

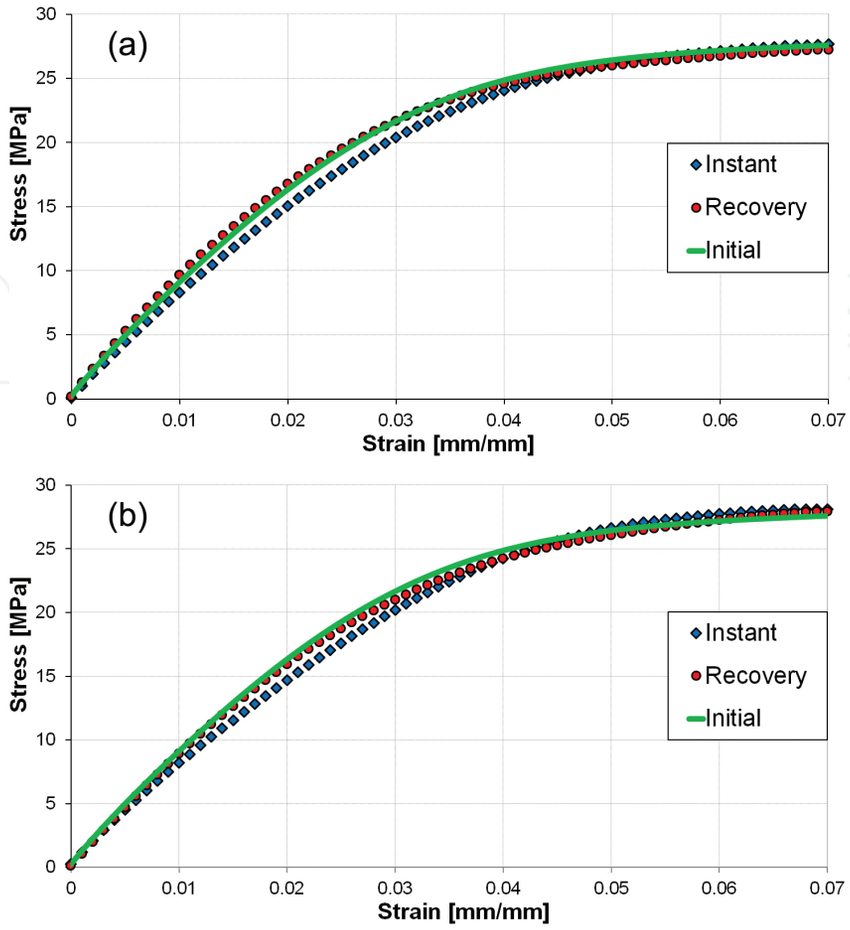

Figure 23. Tensile test comparison for 0.035 (a) and 0.045 mm/mm (b).

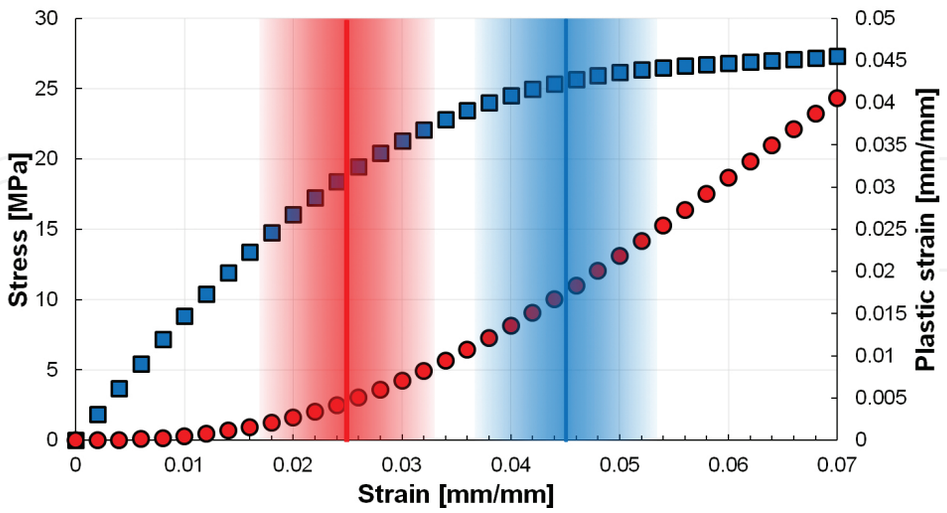

Figure 24. Stresses and plastic strains for reference strain values of 0.025 (vertical red line) and 0.045 mm/mm (vertical blue line) and their correspondent amplitude range (areas with blue gradient and red gradient).

http://dx.doi.org/10.5772/64563

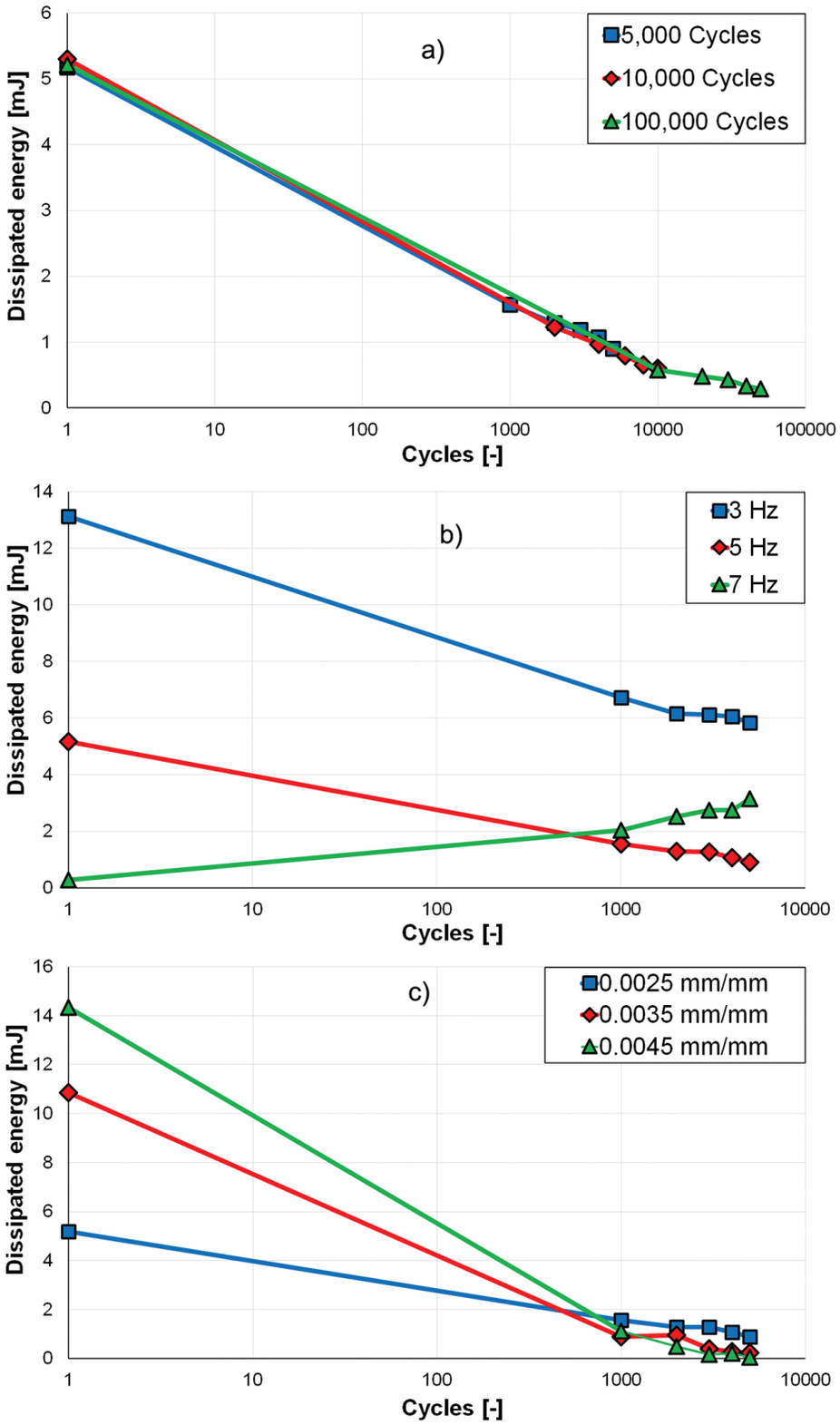

Figure 25. Variation of energy dissipation with cycles for the influence of number of cycles (a), frequency (b) and strain (c).

The same mechanism of deformation determines higher values for the dissipated energy at higher strains, and almost no energy dissipated after 5000 cycles for the tests performed at the highest pre-strain (faster saturation of viscous strain), as seen with the tests performed at varying strains (**Figure 25c**).

Tensile tests show that the LCF test parameters have little influence on the stress-strain response of the material. A slight softening occurred between 0.01- and 0.05-mm/mm deformation in the case of the specimens tested immediately after the fatigue tests, softening that is reverted after the specimen has recovered. It was also observed that, after the LCF tests were completed, when unloading to 0 N, a remnant deformation was observed, ranging from 0.013 to 0.02 mm/mm. Considering that all types of specimens determine similar responses, it can be concluded that no damage was induced to the structure of the material, the apparent softening observed during testing being caused by the accumulation of reversible (viscous) deformations.

This observation is backed by the analysis of the strain variation of the instantaneous elastic moduli variation (which was obtained by dividing the stress increment with the strain increment of the recorded cycles). For all tests, the results are similar, the stiffness of the material increasing as the number of cycles grew (**Figure 26**).

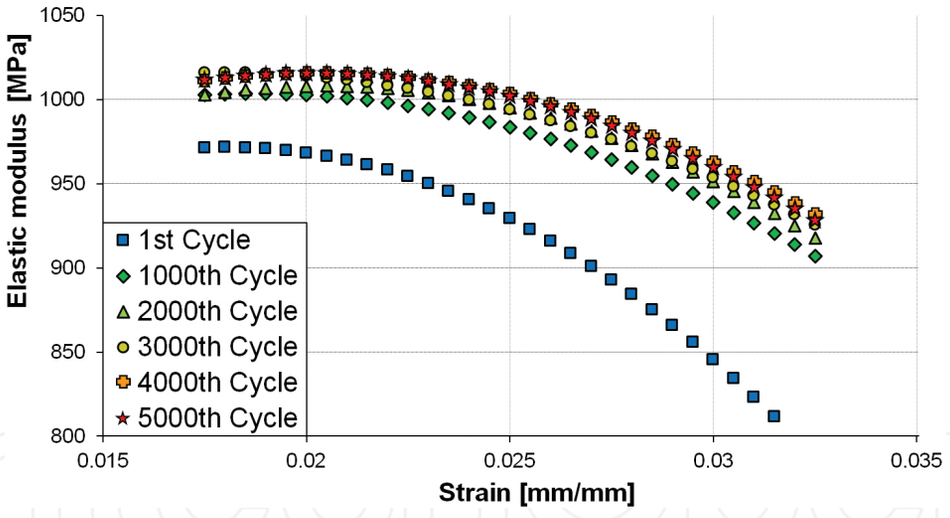

Figure 26. Variation of instant elastic moduli with strain.

To interpret this graph, we need to investigate the stiffness variation with strain, similar to **Figures 5** and **9**. In this case, for the same extensometer opening (LCF tests being performed in strain control), the 5000th cycle determined stiffer responses and lower stresses, compared with the results of the first cycle (**Figure 27**). This happens because, during cyclic loadings, the accumulated viscous strain shifts the loading spectrum towards lower elastic strains. **Figure 28** shows the strain intervals of the first cycle (blue gradient, the blue vertical line being the reference strain) and the equivalent strain interval of the 5000th cycle (red gradient). Overlapped with the stress-strain curve of tests performed on 0.1 s^{-1} (the strain

http://dx.doi.org/10.5772/64563

rate of the 5-Hz tests was 0.075 s^{-1}), it can be observed that values for the stresses and stiffness of both cycles match with the stress and stiffness response of the material [32].

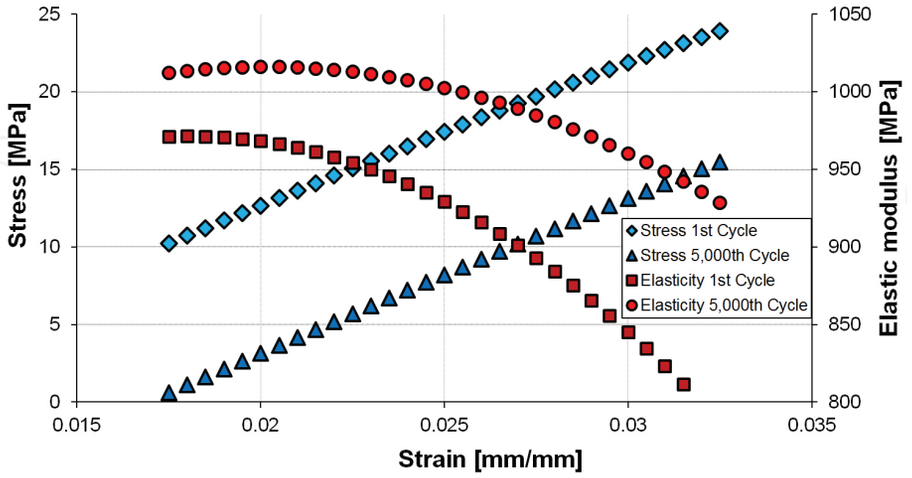

Figure 27. Variation of stress and of the instantaneous elastic modulus with strain for the first cycle and for the 5000th cycle.

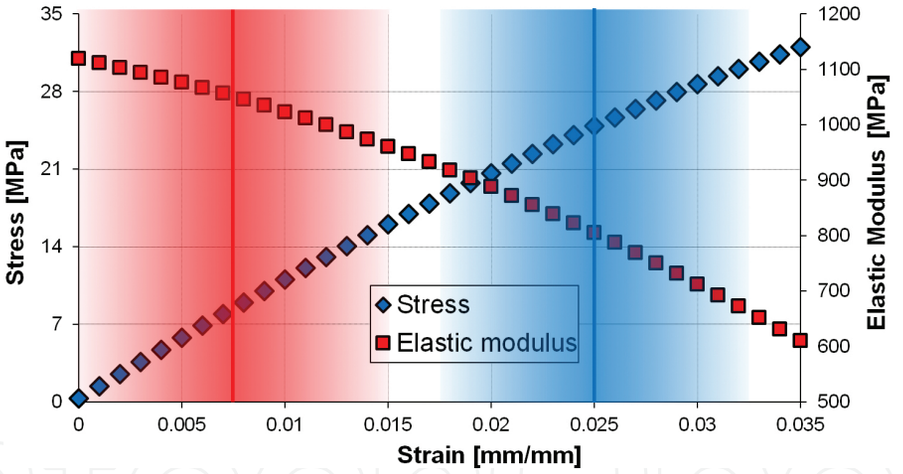

Figure 28. Stress-strain and modulus-strain curves in tension at a 0.1 s-1 strain rate and the deformation interval for the initial cycle (blue gradient) and final cycle (red gradient).

3. Conclusions

This work presents an extensive experimental programme performed on a polyamide compound, in order to determine its non-linear behaviour when subjected to various loading scenarios.

The first set of tests studied the strain-rate dependency of the material with deformation speeds ranging from 0.00028 to 2.8 s^{-1}. Tests were performed in tension and highlighted the strong

influence of this parameter on the material's strength and stiffness. Going further than the low-speed tests, creep tests were performed in order to determine the material softening with time. The tensile compliance increased drastically in the first few minutes of the tests and even though it decreased significantly after 7 h, no plateau (saturation of the viscous strain) was observed after 24 h.

Temperature-dependency tests were performed in order to determine the mechanical properties of the polyamide in an envelope of temperatures that might occur during service. A substantial difference in behaviour was observed between the tests performed at low temperatures (−25 and 0°C) and the tests performed at high temperatures (23 and 50 °C).

Considering this aspect, temperature-sweep dynamical mechanical analysis tests were performed at 1 and 10 Hz in order to determine the glass transition temperature of the material. As expected, the GTT is situated near the ambient temperature (around 40°C), which might influence the material's response significantly during service.

Regarding the dynamical properties and keeping in mind the deformation range that products manufactured from this material might be subjected to, DMA tests at high strains (up to ~4% deformation) were performed. The dynamic moduli vary with strain as expected and the damping coefficient reaches a plateau when deformations get close to the yield region.

Further insight about the long-term effects of loadings was obtained by performing low-cycle fatigue tests. The experimental programme focused on the influence of the number of cycles, frequency and strain on the mechanical properties of the material. It was concluded that, considering the given test regimes, the magnitude of the plastic deformation was reduced, viscous flow having the main influence on the behaviour of the material.

Author details

Şerban Dan-Andrei

Address all correspondence to: dan.serban@upt.ro

Research Institute for Renewable Energy, Polytechnic University of Timişoara, Timişoara, Romania

References

[1] Sperling L. An Introduction to Physical Polymer Science. 4th ed. Wiley-Interscience; Hoboken, New Jersey, USA, 2006.

[2] Strobl G. The Physics of Polymers. Springer; Berlin, Germany, 2007.

[3] Kumar A, Gupta R. Fundamentals of Polymer Engineering. 2nd ed. Marcel Dekker Inc.; New York, NY, USA, 2003.

[4] Bower D. An Introduction to Polymer Physics. Cambridge University Press; New York, NY, USA, 2002.

[5] Brinson H, Brinson L. Polymer Engineering Science and Viscoelasticity: An Introduction. Springer Science; New York, NY, USA, 2008.

[6] Shaw M, MacKnight W. Introduction to Polymer Viscoelasticity. Wiley-Interscience; Hoboken, New Jersey, USA, 2005.

[7] Şerban DA, Marşavina L, Silberschmidt VV. Behaviour of semi-crystalline thermoplastic polymers: Experimental studies and simulations. Computational Material Science. 2012;52:139–146.

[8] Şerban DA, Weber G, Marşavina L, Silberschmidt VV, Hufenbach W. Tensile properties of semi-crystalline thermoplastic polymers: Effects of temperature and strain rates. Polymer Testing. 2013;32:413–425.

[9] Bonet J, Wood R. Nonlinear Continuum Mechanics for Finite Element Analysis. Cambridge University Press; New York, NY, USA, 1997.

[10] Yeoh O. Some forms of the strain energy function for rubber. Rubber Chemistry and Technology. 1993;66:754–771.

[11] Ogden R. Large deformation isotropic elasticity—on the correlation of theory and experimental for incompressible rubber like solids. Proceedings of the Royal Society. 1972;326:565–584.

[12] Arruda E, Boyce M. A three-dimensional constitutive model for the large stretch behaviour of rubber elastic materials. Journal of Mechanics & Physics of Solids. 1993;41:389–411.

[13] Marlow R. A general first invariant hyperelastic constitutive model. Constitutive Models for Rubber. 2003; 157–160.

[14] Drozdov A, Christiansen J. Finite viscoplasticity of semicrystalline polymers. Archive of Applied Mechanics. 2003;72:779–803.

[15] Drozdov A, Christiansen J. Cyclic viscoplasticity of carbon black-filled thermoplastic elastomers: Experiments and modelling. Computational Materials Science. 2009;45:398–406.

[16] Drozdov A. Cyclic viscoelastoplasticity and low-cycle fatigue of polymer composites. International Journal of Solids and Structures. 2011;48:2026–2040.

[17] Presidential Commission on the Space Shuttle Challenger Accident. Report to the President of the Presidential Commission on the Space Shuttle Challenger Accident.

National Aeronautics and Space Administration and the Government Printing Office, Washington, D.C., 1986.

[18] ISO 527. Plastics—Determination of Tensile Properties. International Organization for Standardization, Geneva, Switzerland, 1996.

[19] Xiao X. Dynamic tensile testing of plastic materials. Polymer Testing. 2008;27:164–178.

[20] Şerban DA, Marşavina L, Silberschmidt VV. Response of semi-crystalline thermoplastic polymers to dynamic loading: A finite element study. Computational Material Science. 2012;64:116–121.

[21] Şerban DA, Hanson H, Marşavina L, Silberschmidt VV. Viscoelastic properties of semi-crystalline thermoplastic polymers: dynamic analysis and creep. Solid State Phenomena. 2011;188:211–218.

[22] Dunne F, Petrinic N. Introduction to Computational Plasticity. Oxford University Press; New York, NY, USA, 2006.

[23] Rees D. Basic Engineering Plasticity. Elsevier; Oxford, United Kingdom, 2006.

[24] Cantournet S, Desmorat D, Besson J. Mullins Effect and cyclic stress softening of filled elastomers by internal sliding and friction thermodynamics model. International Journal of Solids and Structures. 2009;46:2255–2264.

[25] Drozdov A. Mullins' effect in thermoplastic elastomers: Experiments and modeling. Mechanics Research Communications. 2009;36:437–443.

[26] Diani J, Fayolle B, Gilormini P. A review on the Mullins effect. European Polymer Journal. 2009;45:601–612.

[27] Diani J, Brieu M, Vacherand J. A damage directional constitutive model for Mullins effect with permanent set and induced anisotropy. European Journal of Mechanics A/Solids. 2006;25:483–496.

[28] Drozdov A. Mullins' effect in semicrystalline polymers. International Journal of Solids and Structures. 2009;46:3336–3345.

[29] Drozdov A, Dusunceli N. Mullins-type phenomena in polypropylene. International Journal of Applied Mathematics and Mechanics. 2012;8:82–98.

[30] Dorfmann A, Ogden R. A constitutive model for the Mullins effect with permanent set in particle-reinforced rubber. International Journal of Solids and Structures. 2004;41:1855–1878.

[31] Şerban DA, Marşavina L, Culea L, Silberschmidt VV. Experimental determination of Mullins effect in semi-crystalline thermoplastic polymers. Acta Technica Napocensis. 2010, Volume 53, pages 317–323.

[32] Şerban DA, Marşavina L, Modler N. Low-cycle fatigue behaviour of polyamides. Fatigue and Fracture of Engineering Materials and Structures. 2015;38:1383–1394.